Sensors for the CDF Run2b Silicon Detector

T. Akimoto, M. Aoki, P. Azzi, N. Bacchetta, S. Behari, D. Benjamin, D. Bisello, G. Bolla, P. Booth, D. Bortoletto, A. Burghard, G. Busetto, S. Cabrera, A. Canepa, G. Cardoso, M. Chertok, C. I. Ciobanu, P. Cooke, G. Derylo, I. Fang, E.J. Feng, J.P. Fernandez, B. Flaugher, J. Freeman, L. Galtieri, J. Galyardt, M. Garcia-Sciveres, G. Giurgiu, I. Gorelov, C. Haber, D. Hale, K. Hara, R. Harr, C. Hill, M. Hoeferkamp, J. Hoff, B. Holbrook, S.C. Hong, M. Hrycyk, T. H. Hsiung, J. Incandela, E.J. Jeon, K.K. Joo, T. Junk, H. Kahkola, S. Karjalainen, S. Kim, K. Kobayashi, D.J. Kong, B. Krieger, M. Kruse, S. Kyre, R. Lander, T. Landry, R. Lauhakangas, J. Lee, R.-S. Lu, P.J. Lujan, P. Lukens, E. Mandelli, C. Manea, P. Maksimovic, P. Merkel, S.N. Min, S. Moccia, Y. Nakamura, I. Nakano, D. Naoumov, T. Nelson, B. Nord, J. Novak, T. Okusawa, R. Orava, Y. Orlov, K. Osterberg, D. Pantano, V. Pavlicek, D. Pellett, J. Pursley, P. Riipinen, B. Schuyler, S. Seidel, A. Shenai, A. Soha, D. Stuart, R. Tanaka, M. Tavi, H. Von der Lippe, J.-P. Walder, Z. Wang, P. Watje, M. Weber, W. Wester, K. Yamamoto, Y.C.Yang, W. Yao, W. Yao, R. Yarema, H. Yoshitama, J.C. Yun, F. Zetti, T. Zimmerman, S. Zimmermann, S. Zucchell

***Abstract*-- We describe the characteristics of silicon microstrip sensors fabricated by Hamamatsu Photonics for the CDF Run 2b silicon detector. A total of 953 sensors, including 117 sensors from prototyping, have been produced and tested for electrical and mechanical properties. Five sensors were irradiated with neutrons up to 1.4$\times$ 10^{14} n/cm^{2}, as a part of the sensor quality assurance program. The electrical and mechanical characteristics are found to be superior in all aspects and fulfill our specifications. We comment on charge-up susceptibility of the sensors that employ <100> wafers.**

Manuscript received November 15, 2003. This work was supported in part by the Japanese Ministry of Education, Culture, Sports, Science and Technology under Grant in Aid for Scientific Research (KAKENHI) on Priority Areas, 13047101, and operated by Universities Research Association Inc. under Contract No.DE-AC02-76CH03000 with the United States Department of Energy..

T. Akimoto, M. Aoki, K. Hara (contact e-mail: hara@px.tsukuba.ac.jp), S. Kim, Y. Nakamura, and H. Yoshitama are with University of Tsukuba, Tsukuba, Ibaraki 305-8571, Japan. P. Azzi, N. Bacchetta, D. Bisello, G. Busetto, C. Manea, D. Pantano, and Z. Wang are with Universita' di Padova and INFN-Padova, Italy. S. Behari, P. Maksimovic, B. Nord, J. Pursley, and B. Schuyler are with Johns Hopkins University, Baltimore, MD 21218F. D. Benjamin, S. Cabrera, and M. Kruse are with Duke University, Durham, NC 27708. G. Bolla, D. Bortoletto, A. Canepa, J.P. Fernandez, and J. Novak are with Purdue University, West Lafayette, IN 47907. P. Booth and P. Cooke are with University of Liverpool, Liverpool L69 7ZE England. A. Burghard, I. Gorelov, M. Hoeferkamp, D. Naoumov, S. Seidel, and P. Watje are with University of New Mexico, Albuquerque, NM 87131. G. Cardoso, G. Derylo, I. Fang, B. Flaugher, J. Hoff, M. Hrycyk, P. Lukens, P. Merkel, S. Moccia, T. Nelson, Y. Orlov, V. Pavlicek, A. Shenai, W. Wester, R. Yarema, J.C. Yun, and T. Zimmerman are with Fermilab, Batavia, IL 60510. M. Chertok, B. Holbrook, R. Lander, T. Landry, D. Pellett, A. Soha, and W. Yao are with University of California, Davis, CA 95616. C. I. Ciobanu, T. H. Hsiung, and T. Junk are with University of Illinois at Urbana-Champaign, Urbana, IL 61801. E.J. Feng, J. Freeman, L. Galtieri, M. Garcia-Sciveres, C. Haber, B. Krieger, P.J. Lujan, E. Mandelli, H. Von der Lippe, J.-P. Walder, M. Weber, W. Yao, F. Zetti, and S. Zimmermann are with Lawrence Berkeley Laboratory, Berkeley, CA 94720. J. Galyardt and G. Giurgiu are with Carnegie Mellon University, Pittsburgh, PA 15213. D. Hale, C. Hill, J. Incandela, S. Kyre, and D. Stuart are with University of California, Santa Barbara, CA 93160. R. Harr is with Wayne State University, Detroit, MI 48202. S.C. Hong, E.J. Jeon, K.K. Joo, D.J. Kong, J. Lee, S.N. Min, and Y.C.Yang are with Kyungpook National University, Daegu, 702-701 Korea. H. Kahkola, S. Karjalainen, and M. Tavi are with Academia Sinica, Taipei, Taiwan 11529, Republic of China. K. Kobayashi, I. Nakano, and R. Tanaka are with Okayama University, Okayama 700-8530, Japan. R. Lauhakangas, R. Orava, K. Osterberg, and P. Riipinen are with Pohjois-Savo Polytechnic (PSPT), Kuopio, Finland. R.-S. Lu is with University of Helsinki and Helsinki Institute of Physics, Finland. T. Okusawa and K. Yamamoto are with Osaka City University, Osaka 558-8585, Japan. S. Zucchell is with Universita' di Bologna and INFN-Bologna, Italy.

I. INTRODUCTION

THE CDF collaboration has designed a new silicon tracker system [1] for Tevatron Collider Run 2b. The system is a six double-layer device located between 2.1 cm and 17 cm radius, consisting of about 2300 single sided silicon microstrip sensors. The whole detector is divided into an inner layer (L0) with 144 axial sensors and five outer layers (L1 to L5) with 1512 axial and 648 1.2-degree stereo sensors. In the following we report on the outer sensors results, as the small fraction of the inner sensors are similar although smaller in size (78.5 mm$\times$ 15 mm) and with a finer pitch (25 μm with alternate readout strips). Details of the L0 design can be found in [2].

The outer layers are built out of compact stave structures [3]. Each stave consists of twelve silicon sensors. Layers 1 and 5 have axial sensors on both sides, while Layers 2 to 4 have axial sensors on one side and stereo on the other side. The double axial layers, L1 and L5, provide efficiently unambiguous anchor hit points that can be used for L0 hit search and for track extrapolation to the outer tracking system. The silicon sensors are glued to a rohacell structure sandwiched by carbon-fiber (CF) sheets and internal bus cables. The readout hybrids are glued directly on the silicon sensors. The cooling tube, embedded in the rohacell, sinks efficiently the heat generated in the sensors after receiving radiation and in ASIC chips on the hybrids: The innermost sensors are designed to operate at –5°C. Such staves construct a 66 cm long cylindrical barrel

structure with each end supported by a CF bulkhead. Fig. 1 shows an endview of the barrel. Two barrels, each containing 90 staves, are arranged along the beamline (in z) covering the interaction region to $|\eta|<2$ with a small gap between the barrels at z=0. Details of the stave design are given in [1, 3].

The sensors are fabricated by Hamamatsu Photonics (HPK), see Fig. 2. The sensors are p^+ microstrips on n-bulk with 512 AC-coupled readout strips. An un-read strip, called an intermediate strip, is located between readout strips, which enhances the position resolution by charge division. The dimensions of axial (stereo) sensors are 40.6 (41.1) mm wide and 96.4 mm long so that two sensors can be taken from a 6" wafer. Table I summarizes the main specifications. We employed the HPK standard 6" wafer of 320-μm thickness and with <100> crystal orientation.

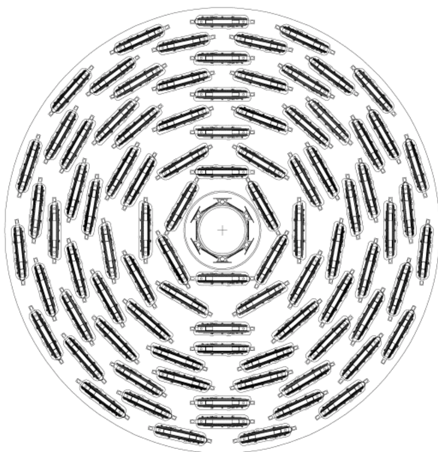

Fig. 1. Cross sectional view of the new silicon system, consisting of 90 staves in five layers, and a beam-pipe L0 layer (16 cm outer radius). Two sets are aligned in the beam direction covering 120 cm long region.

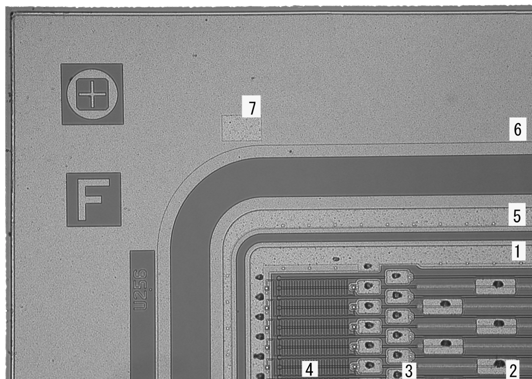

Fig. 2. Photograph of the sensor corner area: (1) bias ring, (2) AC pads, (3) DC pads for readout and intermediate strips, (4) bias resistors, (5) guard ring, (6) edge ring, and (7) Nsub pad, which is connected to the bulk. The distance of the bias ring to the scribed edge is 1 mm.

We require that the sensors are radiation hard to 1.4×10^{14} 1-MeV equivalent neutrons per square centimeters, the fluence being estimated to correspond to 30 fb^{-1} of Tevatron luminosity at the innermost layer. Specific requirements for radiation hardness of these sensors are the high voltage operation in excess of 500 V (this might be necessary after a large radiation dose) and the relatively high starting depletion voltage with a minimum value set at 100 V.

The system requires 1512 axial and 648 stereo sensors. We report on characteristics of 953 delivered sensors. First, we describe the electrical properties of the sensors. Five axial sensors were irradiated with neutrons up to1.4×10^{14} n/cm^2. The characteristics of these sensors are also given. We observed some charge-up susceptibility and studied to understand its characteristics. Mechanical properties are also studied. Finally, we summarize the results.

Table I. Main specifications of axial and stereo sensors

Specifications	Axial	Stereo
Wafer	<100>; 320±15μm thickness; < 130μm warp	
Dimensions	40.55 x 96.392 mm	41.10 x 96.392 mm
Full depletion voltage	100 V < Vdep < 250 V	
Leakage current	< 2 μA at 20°C and at 500 V	
Number of strips	512 readout and 513 intermediate strips	
Strip widths	8 μm implant and 14 μm Al electrode	
Readout strip pitch (angle)	75 μm (0°)	80 μm (1.2°)
Coupling capacitor	capacitance > 120 pF; breakdown voltage >100 V	
Interstrip capacitance	< 1.2 pF/cm	
Poly silicon resistance	1.5±0.5 MΩ	
Defective strip fraction	< 1%	

II. Electrical Properties

A. *General Quality Assurance (QA) Procedure*

Hamamatsu Photonics performed intensive QA tests: I-V, C-V, AC-pad scan, and DC-pad scan. The AC-pad scan classifies defective strips as "AC Open" (the aluminum strip has a break), and "AC Short" (neighboring aluminum strips are shorted). The DC-pad scan reports "Open" (the implant strip has a break), "Short" (neighboring implant strips are shorted), "Leaky" (the strip current is large), and "Bad Isolation" (the interstrip resistance is too small).

We have performed additional tests in order to verify the HPK test results and to evaluate the electrical characteristics in further detail. The tests are:

1. I-V curve: Total leakage current was measured up to 1000 V bias at a step of 10 V.
2. I-V curve stability: I-V curves were measured every 30 min at least for 10 times, typically for 30 times. The bias voltage between the I-V measurements was set at 500 V.
3. C-V curve: Total capacitance was measured as a function of bias voltage. The curve was used to extract the full depletion voltage.

4. AC scan: Oxide coupling capacitance, and equivalent series resistance (implant and bias resistance) were measured for each readout strip with an LCR meter. Also, the leakage current was measured when 100 V was applied across the oxide.
5. DC scan: The leak current of individual strip was measured for the sensor which showed a rapid increase in leakage current, or micro-discharge [4]. The bias was set above the micro-discharge onset voltage.
6. Interstrip isolation: The interstrip resistance was measured with applying voltages (−1 to +1V) to the neighboring intermediate DC pads and measuring the current emerging from the readout DC pad under test
7. Interstrip capacitance: The capacitance between the neighboring AC pads was measured. Other strips were floating to the ground.

We measured I-V and C-V characteristics for all the sensors (except for some prototype sensors). The AC scan and IV stability tests were performed on a sampling basis. The rest of the tests were made less frequently: In particular they were performed to diagnose the sensors that showed deviated results from the expectation.

B. *I-V characteristics*

The I-V curve is relatively easy to measure, yet providing overall view on the sensor quality. In Fig. 3 we show typical I-V curves of a subset of the sensors. The measured leakage current values were normalized at 20°C while the test bench temperature was in the range 26 to 30°C. The leakage current is quite small and most of the sensors do not show any significant micro-discharge up to 1000 V we measured[1]. There are two sensors in this sample of 116 sensors, which show micro-discharge with the onset voltages of around 800 and 900 V. The leakage currents at 500 and 950 V are shown in Fig. 4 for all 953 sensors.

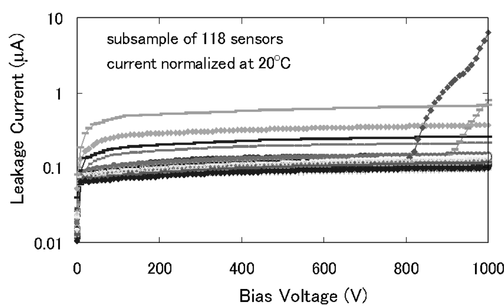

Fig. 3. Typical I-V curves (curves for 116 sensors are overlaid).

The leakage current is typically 0.1 μA. We set our leakage current requirement to be less than 2 μA at 500 V in order to insure that no single readout strip has a leakage current exceeding ~1μA as this would degrade the noise performance. All the sensors fulfilled this specification. In addition, 97% of the sensors showed leakage current below 0.5 μA even at 950 V. HPK has realized this superior performance by employing a single guard-ring structure with 1 mm distance between the scribed edge and the sensitive area (see Fig. 2).

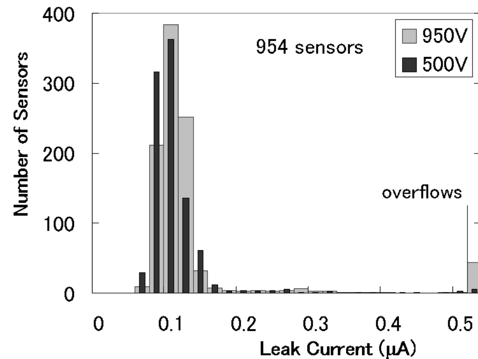

Fig. 4. Leakage currents at 500 and 950 V for all 954 sensors. The numbers exceeding 0.5 μA are given in extremely right bin

For the sensors that show micro-discharge, we have verified that the micro-discharge is caused at a single or a few strips by measuring the individual strip leakage (DC scan). It would be also possible to use these sensors if such strips are disconnected from the readout.

C. *Stability of I-V curves*

The I-V stability was measured for 42 sampled sensors. This test is motivated to monitor the surface quality of the sensor. Between the I-V measurements, the sensors were biased at 500 V for 30 min. The results can be categorized into four types. For most of the sensors (35 sensors), the I-V curves were consistent and stable, as in Fig. 5(a). Two sensors showed stability as in Fig. 5(b), where small micro-discharge developed above 900 V. We found four sensors that showed much significant micro-discharge as shown in Fig. 5(c). Among these, two sensors that showed significant micro-discharge were selected from the initial I-V measurement: the onset voltage increased gradually with time. The other two were good to 1000 V initially but the onset voltage of 600 V showed up within 1 hr. The onset voltage then increased with time, reaching 800 V or higher at the last measurement.

An exceptional behavior was observed for one sensor. The I-V stability is shown in Fig. 5(d). The I-V, initially good to 1000 V, started to become chaotic after 8 hr and finally went into breakdown at 800V after 10 hr. We investigated the cause with an IR camera, and found a discharge hole on the bias-ring. Since we recognized no hint of discharge bridging to nearby structures, the discharge must have occurred towards the bulk substrate probably via some defect in the wafer. The sensor did not recover, indicating the creation of a permanent junction breakdown.

[1] Although our specification is 500 V, we investigated the possibility of operating the same sensor at higher voltages for future applications. Since our initial results were promising up to 1000 V, we chose 1000 V as the maximum to apply.

In summary, most sensors are good to 1000 V, but some created micro-discharge after a time scale of 1 hr. In any case, operation below 500 V should be safe.

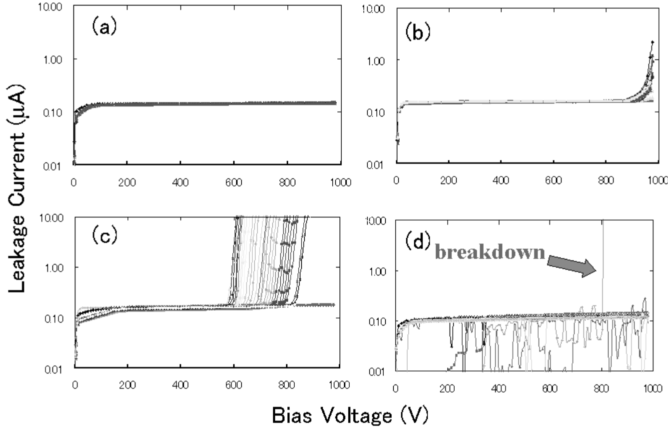

Fig. 5. Classification of I-V stability of 42 sensors. (a) Typical (35 sensors), (b) 2 sensors with small micro-discharge, (c) 4 sensors with significant micro-discharge, and (d) one sensor which showed breakdown at 800 V at 18th time.

D. Full Depletion Voltage

We measured the C-V curves of 908 sensors using an LCR meter with test pulses at 400 Hz and 1 V. We extracted the full depletion voltage as the intercept of two straight lines in a C^{-2} -V plot. The full depletion voltage distributed from 87 V and 165 V, as shown in Fig. 6.

Our depletion voltage specification of 100 V to 250 V is based on the resistivity range from 1.25 to 3.25 kΩcm, a wafer class employed by HPK. Some fraction, 7.7%, of the sensors are found not to maintain the specification: It is excused by HPK that the wafer resistivity is not uniform and applied sampling, three points per wafer, was not enough. Since the requirement, minimum of 100 V, is to prolong the sensor lifetime before inversion, such sensors are safely usable if we place them in the outer layers.

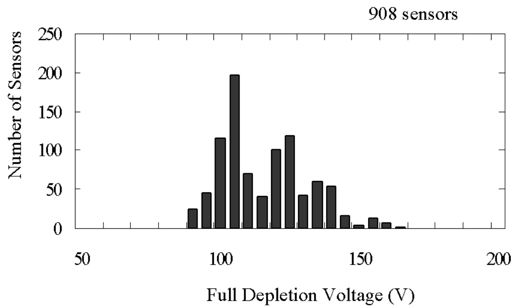

Fig. 6. Distribution of the full depletion voltages.

E. AC scan and Number of Defect Strips

The strip integrity was intensively evaluated by AC scan where the measurement was performed in two steps. Firstly, the capacitance and series resistance were measured by probing between the AC pad and bias-ring with setting the LCR meter at Cs-Rs mode and at 400 Hz. Secondly, a 100 V pulse was applied across the oxide and the leakage current through was measured 1 second after. The capacitance represents the oxide coupling capacitance, and the resistance the sum of the bias resistance and implant electrode resistance. The implant resistance contributes approximately 0.3-0.5 MΩ.

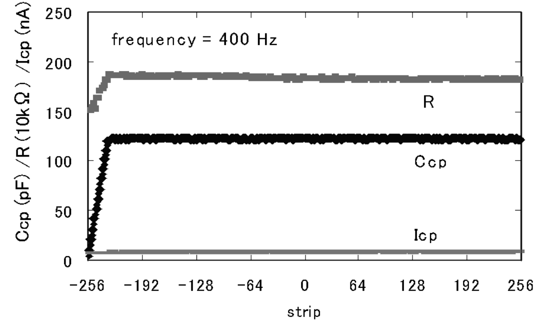

Fig. 7. AC scan result for a stereo sensor. The coupling capacitor Ccp increases with strip length and reaches about 120 pF. The series resistance R, starting from poly-silicon resistance of 1.5 MΩ, reaches about 1.8 MΩ.

AC scan was performed for 49 sensors. The coupling capacitors and resistors were found to be very uniform and defective strips can be easily identified: An example plot is given in Fig. 7 for a stereo sensor, where first 25 strips starting from –256 are shorter due to angle. The leakage current in this plot, about 10 nA, is due to the leakage through the CMOS relays that we used in the apparatus to isolate the LCR inputs from 100 V pulses. This is larger than the leakage through genuine coupling capacitors, but is much smaller than the leakage when the oxide has a punch-through, 10 μA, which is defined by protection resistors in the system.

With HPK's AC scan, they evaluate various defects by injecting step pulses into the bulk from the backside contact and measuring the signal emerging out from the AC pad, thus eliminating use of an LCR meter. No bias is applied in this measurement. One of the purposes of our AC scan is to verify the HPK results.

The 49 sensors we selected have defects reported by HPK. Except for some leaky strips and bad isolation strips, we succeeded to identify all the other defects. Those unidentified defects can be ignored from the following reasons. Large leakage current tends to decrease with time, as described in Section II.C. Also, isolation degradation can be understood as non-permanent charge up, as is described in Section IV.

We created a couple of new damages associated with the probing system manipulation. Such damages are obvious by visual inspection. Apart from them, we have observed six new defects, which were later identified with a microscope as readout implant breaks.

Table II summarizes the number of defect strips measured by HPK. The percentages are given with respect to the total number of (readout or intermediate) strips of 488 thousands. Among these, the fraction of intermediate strip breaks is dominating. The readout implant breaks are substantially fewer, although we expect similar fractions because the both breaks are mostly created by dusts in the process. This apparent discrepancy is explained by that HPK probing is barely sensitive to detect the readout implant opens because of the sensor layout we employed. In our sensor layout, the poly-silicon resistors for readout strips are arranged at the probing side while those for intermediate strips are at opposite side. The opposite side where the hybrid is glued on top is completely passivated, and does not allow probing. Because of this limitation, the readout implant breaks are not detected efficiently by just probing DC pads and bias-ring at the same side, which is not the case for intermediate implants. In Table II we added six readout breaks with the fraction calculated for 49 sensors we measured. The fraction of the readout implant breaks is now comparable with that of intermediate implant breaks. Adding the defects listed in the table, we estimate the fraction of the readout strip defects to 0.04%. The fraction of implant breaks, which would degrade the resolution locally, is 0.05%.

Table II. Numbers and fractions of defect strips measured by HPK. The numbers in brackets are estimations from our measurements (see text).

Total number of strips	488k	
Readout implant break	2[+6]	[0.024%]
Interm. implant break	238	0.049%
Al electrode break	11	0.002%
Al electrode short	18	0.004%
Oxide punchthrough	17	0.003%
Poly-Si break	3	0.001%
Bad isolation	7	0.001%

F. *Other Electrical Properties*

1) *Interstrip Resistance*

We evaluated the interstrip resistance measuring the increase/decrease in the readout strip leakage current when DC voltages ($\pm 1, \pm 0.5$ V) were applied to the two intermediate strips at neighbor. The sensor was biased to 200 V. The four resistance values so obtained were averaged to represent the interstrip resistance. Three axial sensors were measured. One sensor showed resistance of in the 50-200 GΩ range, and other two sensors showed 100-300 GΩ.

2) *Interstrip Capacitance*

We evaluated the interstrip capacitance probing neighboring (readout) AC pads with other Al electrodes at floating and the detector bias at 200 V. The LCR frequency was set to 1 MHz. We have measured the interstrip capacitance of in total 9 axial and 2 stereo sensors. Among 5600 pairs of strips, only two pairs showed irregular values of 5% off the nominal value.

III. PROPERTIES OF IRRADIATED SENSORS

A. *Neutron Irradiation*

Radiation damage of silicon sensors has been studied intensively for the application to *e.g.* LHC experiments. Although radiation in CDF is composed of various hadrons, we irradiated 5 sensors with neutrons at MNRC Irradiation Facility at UC Davis in order to verify that our sensors are radiation hard to the similar level as previously reported [5]. Three of the sensors received 1.4×10^{14} cm^{-2} 1-MeV neutron equivalent fluence and the other two 0.7×10^{14} cm^{-2} 1-MeV equivalent [6]. The actual doses were calibrated by sulfur activation to 1.40×10^{14} and to 0.67×10^{14} n/cm^2 with typical uncertainty of 10%. The irradiation time was 69 min in total. No sensor bias was applied and no temperature control was attempted during the irradiation.

Right after the irradiation the sensors were stored at -7°C. The sensor temperature was then increased for certain periods so that the beneficial annealing is almost complete hence the full depletion voltage at the minimum.

B. *Total Leakage Current and Full Depletion Voltage*

Fig. 8 shows the I-V curves of the irradiated sensors. The current is normalized at 20°C. The sensors do not cause any micro-discharge up to 1 kV and show clear shoulders indicating that dominating is the leakage current through the bulk.

The measurement of full depletion voltage is strongly affected by high leakage current and therefore was performed in the environmental chamber at -25°C. The full depletion voltages derived from C^{-2}-V plots (an example plot is given in the inset in Fig. 11) ranged from 128 to 130 V for the sensors irradiated to 1.4×10^{14} n/cm^2, and about 50 V for the sensors irradiated to 0.7×10^{14} n/cm^2. These values are consistent with previous measurements [5], which predict that the full depletion voltage be around 120 V and 40 V, respectively.

The damage constant α is expressed by $\alpha = \Delta I/(V\phi)$, where ϕ is the neutron fluence, ΔI the increase in the total leakage current measured at the full depletion voltage, and V the volume of the sensor. Previous studies show that the leakage current of irradiated sensors decreases (anneals) with time. Because of this feature and temperature dependence of the leakage current, α is calculated after the annealing is almost completed and at 20°C. Systematic study of the annealing phenomena is available such as from Rose Collaboration [5]. At room temperatures, the current decreases substantially within a month, with α reaching 3×10^{-17} A/cm.

Instead of evaluating the damage constant, we use our results to evaluate the neutron fluence. The evaluated neutron fluence is 1.1×10^{14} n/cm^2 for the nominal of 1.4×10^{14} n/cm^2, and is (0.33-0.64) $\times 10^{14}$ n/cm^2 for 0.7×10^{14} n/cm^2. The present

results prefer somewhat smaller neutron fluence but are in reasonable agreement.

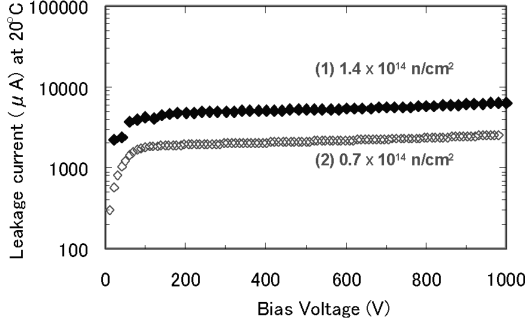

Fig. 8. I-V curves of irradiated sensors. The leakage current is normalized at 20°C. Sensor (1) was measured at 14°C and Sensor (2) at −15°C. Sensor (1) is not completely annealed while Sensor (2) should have completed the initial annealing.

C. Bias Resistance and Interstrip Resistance

The resistances of various sensor components are key properties to evaluate the radiation effect on silicon sensors. The oxide layer accumulates positive charges created by radiation, which degrades among others such as effective bias resistance and interstrip resistance. In the following, we evaluated the degradation using real sensors instead of using test pieces, thus the results represent the effective changes.

Fig. 9a shows the bias dependence of the bias resistance, compared for a particular strip before and after irradiation. Although the resistance saturates below about 100V before irradiation, much larger bias voltage, about 350 V, is required to reach the asymptotic value.

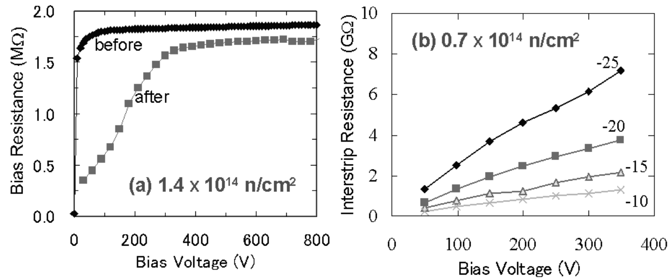

Fig. 9. (a) Bias resistance vs. bias voltage and (b) interstrip resistance vs. bias voltage measured at various temperatures.

Fig. 9b shows the bias dependence of the interstrip resistance. The resistance is substantially degraded: it was greater than 50 GΩ before irradiation. In order to keep the resistance to above 1GΩ, a bias of 250V is required at −10°C.

Although the data are shown for a particular strip (pair), we found that the degradation is very uniform among the strips both for the bias resistance and interstrip resistance.

D. Interstrip Capacitance

Fig. 10 shows the bias dependence of the interstrip capacitance measured for a particular set of neighboring strips for the two sensors irradiated to 1.4×10^{14} n/cm^2. The LCR test signals were at 1 MHz frequency and 5 V amplitude. Although the curves at small bias voltages behave differently due to individual difference, the shoulders around 130 V are consistent with the full depletion voltage. The interstrip capacitance decreases gradually with bias voltage, approaching to asymptotic values consistent with those of non-irradiated sensors. We notice, though, that the bias should be substantially larger than the full depletion voltage to reach the asymptotic value.

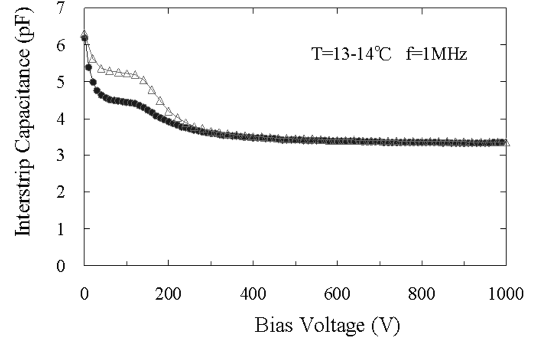

Fig. 10. Interstrip capacitance of irradiated sensors measured as a function of bias. The data are shown for two sensors irradiated to 1.4×10^{14} n/cm^2.

E. Charge collection

The two sensors irradiated to 1.4×10^{14} n/cm^2 were used to construct a module, where a real readout hybrid [3] was attached. This module was illuminated with Nd:YAG laser to investigate the charge collection. The laser wavelength 1064 nm corresponds to the energy slightly above the energy gap of silicon, hence the laser is absorbed almost uniformly along its trajectory. This simulates well the passage of charged particles.

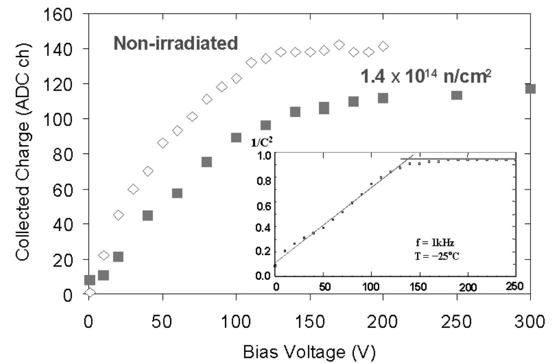

Fig. 11. Charge collection curve of irradiated sensors (filled squares) and of non-irradiated sensors (open diamonds). The inset is C^{-2} –V curve of the irradiated sensor.

Fig. 11 shows the collected charge as a function of the bias voltage. Since the laser spot spreads over a few strips, ADC sum of neighboring strips is plotted. The same curve measured for a non-irradiated module is superimposed in the figure.

The voltage dependence of the charge collection is almost as expected from the C-V curve of the same sensor, which is

shown in the inset in the figure. We though notice that the charge collection of the irradiated module increases even above the full depletion voltage. The deficit in the collected charge can be explained by followings. After irradiation there are active trapping and detrapping centers, which spread the signal arrival time. A tail was actually observed in the collected charge vs. time distribution, indicating that the integration time of the SVX4 chips, 112 ns, is not long enough to collect all the charges. This effect can be mitigated by raising the bias voltage, as we see in Fig. 11.

IV. SENSOR SUSCEPTIBILITY OF CHARGE UP

In the early stage of testing, we often observed the sensor to show degraded performance in a region spreading over about 30 to 50 strips. The symptom is that the coupling capacitances are larger, the series (implant and poly-silicon) resistances are smaller, and interstrip resistances are smaller, which implies that the strip isolation is degraded in the region. After investigation it turned out that the vacuum tweezers used to pick up the sensor caused the charge-up phenomenon. The phenomenon disappears if the sensor is placed back to the envelope provided by HPK.

The wafer orientation we employed is <100>. Because the positive charges trapped at the Si-SiO_2 interface and in the oxide layer are fewer in <100> than in <111>, they attract fewer electrons underneath the interface. Thus, external potentials can create easier a p^+ layer, inversion layer, between the p^+ strips, degrading the strip isolation. MOSFET devices usually use <100> wafers for this reason.

We observed that the charge-up phenomenon could remain at least for a week if the sensor surface is isolated. In our practical sensor application, though, the wire-bonds to the amplifiers, for example, stabilize the Al electrode potential, which should eliminate the inversion layer. In order to verify this hypothesis, we performed the following study.

We created a charge-up sample and wire-bonded three AC pads in the charge-up region to the ground, simulating the connection to the amplifiers. We repeated the AC scan to monitor the recovery. The results are given in Fig. 12. The initial charge-up, as visible in Fig. 12(d), almost recovered 20 h after wire-bonding (Fig. 12(e)). The recovery seems to be somewhat slower at the mid-point between the wire-bonded strips; see the distribution 1 h after (Fig. 12(b)). Therefore, we can conclude that charge-up phenomena, if exist, are to disappear once the sensors are assembled to modules.

From our experience, we are able to diminish the creation of charge-up if we eliminate use of vacuum tweezers. Also we find that the charge-up susceptibility degrades with time: we tried to charge-up the sensors intentionally, but it was hard for the samples 1 month after the delivery. Our hypothesis is that the sensor accumulates positive charges in the oxide layer in this period and became resistive against creation of inversion layer.

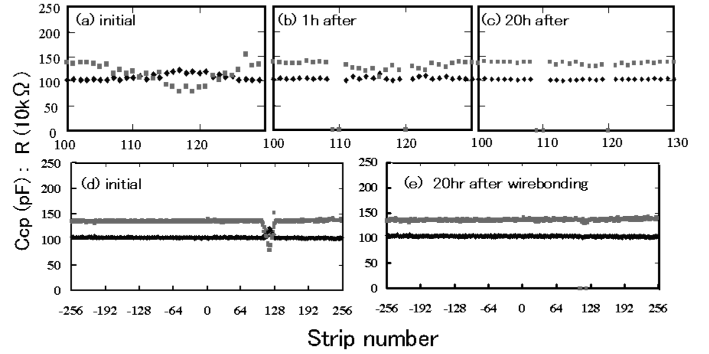

Fig. 12. AC scan results for charge-up study. (d) Initial distribution where strips 105 to 135 show irregular coupling capacitance (100 pF nominal) and series resistance (1.4 MΩ nominal). (a) Expanded plot of the charge-up region. (b) Enlarged plot 1 h after strips 109, 110 and 120 are wire-bonded. (c) Expanded and (e) entire distributions 20 h after. LCR frequency is 1 kHz.

V. MECHANICAL PRECISIONS

The following mechanical precisions were measured for sampled sensors with a measuring microscope, which has a reproducibility of about 2 μm horizontally and 3 μm vertically.

A. *Wafer thickness*

The wafer thickness was measured for 78 sensors at the center of shorter sides. The sensors were placed vertically on a stage under the microscope. The central value was 320.4 μm, with the distribution shown in Fig. 13. The spread is much smaller than the precision quoted by HPK, 15 μm. The thickness difference at the two shorter sides of the same sensor was at maximum 5 μm.

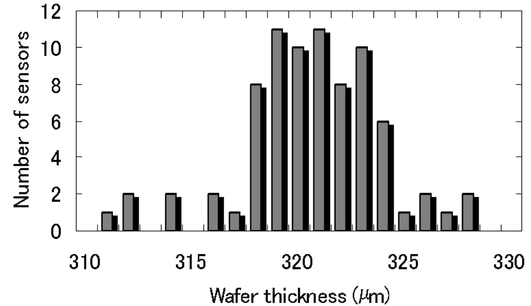

Fig. 13. Distribution of the detector thickness.

B. *Edge Cut Precision*

The distance between the fiducial marks to the edge was measured at the four corners of 44 sampled sensors. The nominal distance is 330 μm. The distance distributed from 323 to 335 μm along the longer side and from 326 to 335 μm along the shorter side. The edge cut precision was better than 7 μm, while the precision quoted by HPK is 20 μm.

C. *Sensor Planarity*

The sensors tend to be bowed due to different thermal expansions between SiO_2 and Si: They are flat at high temperature when processed. The bow is more significant for single-sided sensors than for double-sided sensors.

The planarity was measured on 1 cm grids. Typical profile is given in Fig. 14, where the three corner data are used to define the reference plane and the deviations to it are plotted. The positive deviations mean that the sensor is bowed with the strips on the convex side. The profile is generally universal among the different sensors.

In order to increase the statistics, the height at the sensor center was measured with the microscope with respect to the heights at the fiducials at the four corners. The deviations distributed 80 to 100 μm for 11 axial sensors and 55 to 90 μm for 11 stereo sensors. The difference could be qualitatively explained by that the stereo sensors are wider then axial sensors. The twists, deviations of the 4th fiducial height which was not used to define the reference plane, distributed from –6 to 21 μm for the 22 samples.

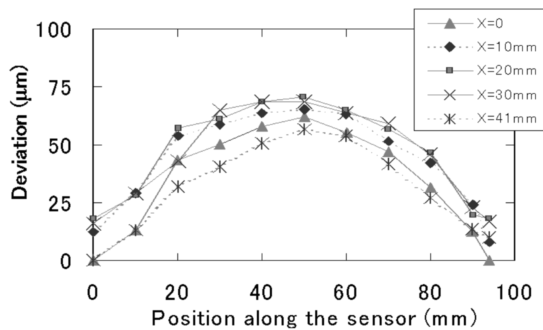

Fig. 14. Height profile of a stereo sensor measured on 1 cm grids.

VI. CONCLUSION

We evaluated the electrical and mechanical properties of microstrip sensors designed for the CDF Run2b silicon detector.

The leakage current is small (0.1 μA typically) and most sensors show no breakdown up to 1000 V. The fraction of defective readout channels is estimated to 0.04%. The coupling capacitance, bias resistance and other electrical values are found to be quite uniform.

We have characterized various electrical parameters of the sensors irradiated with neutrons up to 1.4×10^{14} cm^{-2}. The evolution of the full depletion voltage and increase of the leakage current are consistent with previously known values. Many parameters such as interstrip capacitance, interstrip resistance, and bias resistance are apparently degraded due to charges accumulated in oxide layer and type inversion. We observed that it requires a bias of 250-300V to reach the asymptotic values while the full depletion voltage is evaluated to be around 130 V.

The mechanical precisions, wafer thickness uniformity, edge cut precision and sensor bowing, were measured. All of them are found to be within our specifications.

VII. ACKNOWLEDGMENT

The authors would like to thank K. Yamamura of Hamamatsu Photonics for useful discussions. They also acknowledge MNRC for neutron exposure, D. Newell and H. Ben Liu for providing fluence calibration information.

VIII. REFERENCES

[1] M. Aoki, N. Bacchetta, S. Behari, D. Benjamin, D. Bisello, G. Bolla et al. (CDF Collaboration), "CDF Run IIb Silicon Detector", submitted for Proceedings of 9th Pisa Meeting on Advanced Detectors, La Biodola, Isola d'Elba May 25, 2003; CDF Collaboration, "The CDF IIb Detector: Technical Design Report", FERMILAB-TM-2198 (Feb 2003).

[2] P. Merkel (CDF Collaboration), "CDF Run IIb Silicon: The New Innermost Layer", submitted for IEEE NSS/MIC Conference, Portland, USA, October 19, 2003.

[3] R.-S. Lu (CDF Collaboration), "Stave Design and Testing of SVXIIb of CDF at Fermilab", submitted for IEEE NSS/MIC Conference, Portland, USA, October 19, 2003; M.M. Weber (CDF Collaboration), "Electrical Performance and Dead-timeless Operation of "Staves" for the New CDF Silicon Detector", *ibid*; C. Cardoso (CDF Collaboration), "Polyimide and BeO Mini Portcard Performance", *ibid.*

[4] T. Ohsugi, Y. Iwata, H. Ohyama, T. Ohmoto, M. Yoshikawa, T. Handa et al, "Micro-discharge at strip edge of silicon microstrip sensors", Nucl. Instrum. Methods, vol. A 383, p. 116, 1996.

[5] G. Lindstroem, M. Ahmed, S. Albergo, P. Allport, D. Anderson, L. Andricek et al. (ROSE Collaboration), "Radiation hard silicon detectors – developments by the RD48 (ROSE) collaboration", Nucl. Instrum. Methods, vol. A466, p.308, 2001.

[6] The 1-MeV equivalent fluence was calculated based on ASTM E722 report on "KERMA" (The total kinetic energy release in silicon matter) factors for silicon.